This article has been accepted for publication in a future issue of this journal, but has not been fully edited. Content may change prior to final publication. Citation information: DOI 10.1109/TIE.2020.2984993, IEEE Transactions on Industrial Electronics

Model-Free Energy Management System for Hybrid AC/DC Microgrids

***Abstract*—A hybrid AC/DC microgrid combines the benefits of AC and DC power systems. It provides high efficiency and is compatible with conventional AC distribution network. This paper proposes a centralized energy management approach to perform coordinated control on a hybrid AC/DC microgrid as a single-controllable entity. The central controller relies on low-bandwidth communication channels and is aimed at achieving *1)* proportional power sharing among energy storage units located in both DC and AC sides of the microgrid, *2)* state-of-charge equalization of the energy storage units, *3)* grid power flow control, *4)* plug-and-play capability, and *5)* operation in grid-connected and islanded modes through an interlinking utility interface converter. The state-of-charge equalization method guarantees uniform operation of the energy storage units during both charge and discharge modes considering typical operational transients. Finally, the proposed model-free approach is evaluated experimentally through a laboratory-scale hybrid AC/DC microgrid in different operational conditions in both grid-connected and islanded operating modes.**

***Index Terms*—Hybrid AC/DC microgrid, power-based control, energy storage, power sharing, hierarchical control**

I. Introduction

The growth of renewable energy sources (RESs), energy storage units (ESUs), and modern loads as electric vehicles into the distribution power systems has challenged the grid interconnection in terms of efficiency, reliability and power quality. Regarding the power quality issues, the typical limits of hosting capacity are overvoltage, overload of conductors, and voltage unbalance [1], [2]. In this context, a microgrid (MG) shows itself as a feasible model to enable the interconnection of multiple RESs, ESUs and loads in a same cluster ensuring dispatchability, reliability and stability of the overall system contributing to enhance the hosting capacity of distribution grids and then increasing the amount of distributed energy resources (DERs) integrated into the power system [3].

MGs can be distinguished between AC and DC configurations; and each one requires a proper grid-interactive converter at the point of common coupling (PCC). The AC MG inherits the natural compatibility with conventional equipment since the distribution power system is also AC. On the other hand, DC MG shows high efficiency for the integration of renewables and for supplying electronic loads, since it requires fewer energy conversion stages than AC MG [4]. To take advantage of both configurations, hybrid AC/DC MGs appear as a promising alternative for modern power systems. The main challenge of hybrid AC/DC MGs is to design a proper power management strategy to deal with the coexistence of AC and DC subgrids, achieving fully dispatchable grid power flow, with state-of-charge (SoC) balancing and a stable and reliable operation [5].

The AC and DC subgrids are coupled through an interlinking converter (IC), which is also used to interface the hybrid AC/DC MG to the mains. Such converter creates a path for power flow exchange between both sides, and guarantees seamless transition between grid-connected and islanded operating modes. Besides, it is desirable that the IC provides: grid power flow control, grid-forming performance, active filtering functionality, and low-voltage ride through capabilities. Therefore, a suitable control strategy to coordinate the operation of the IC and the multiple DERs scattered throughout the AC and DC subgrids must be defined.

The power management of MGs is usually performed by means of a hierarchical control. This approach is based on the ISA-95 standard and can be split into primary, secondary and tertiary control levels, depending on the time scale that the tasks are executed and the setting of the control loop implementation [6]. In [7] a power management system for a hybrid AC/DC MG is proposed using droop controllers to achieve proportional power sharing in the primary control level, and a centralized controller, in the secondary level, to achieve an accurate energy management of the MG. The main contributions are proportional power sharing among the parallel DERs, bidirectional operation of the IC, and a centralized controller that does not depend on previous knowledge of DERs control laws, relying on a low-bandwidth communication channel. It has been proved that delays until 1 second do not cause instability. However, the islanded operation has not been considered, neither ESUs.

In [8] is proposed a two-stage modified droop method for the bidirectional power control of the IC during different operating modes of a hybrid AC/DC MG. The proposed method considers the MG as a single entity capable of operating in both grid-connected and islanded modes. It accomplishes bidirectional power flow through the IC, and proportional power sharing among DERs. However, the control method depends on previous knowledge of the MG parameters.

In [9] a single-phase IC transfers active power between DC and AC subgrids, and concomitantly provides ancillary services such as reactive power support, harmonic mitigation and grid-forming capability. An energy management system (EMS) provides functionalities such as load shedding and de-tuning maximum power point (MPP) operation of PV. Battery banks and supercapacitor packs are considered as ESUs; however, they do not operate in a coordinated manner and SoC equalization among them is not attained.

The authors of [10] propose a distributed control for autonomous operation of a hybrid AC/DC MG. Distributed ESUs are considered and located in a DC storage bus interconnected

This article has been accepted for publication in a future issue of this journal, but has not been fully edited. Content may change prior to final publication. Citation information: DOI 10.1109/TIE.2020.2984993, IEEE Transactions on Industrial Electronics

to the DC link of the IC. A fully decentralized control based on droop control is implemented locally to achieve power sharing in each subgrid, and then a global power sharing combining the droop characteristics of each subgrid sets the power flow through the IC. ESUs operate proportionally to their individual SoC value and power capacity. The IC regulates the bidirectional power flow between AC and DC subgrids, but neither grid power flow is controlled, nor islanded operation mode is considered.

The authors of [11] propose a hybrid AC/DC MG endowed with one ESU in each subgrid: AC and DC. In grid-connected mode, both ESUs in AC and DC subgrids operate in constant power mode. Whereas during islanded operation, a $SoC - f$ droop control in the AC ESU regulates the AC frequency, and a $SoC - v$ droop control in the DC ESU regulates the DC bus voltage. However, the addressed method does not provide SoC equalization of ESUs located in both AC and DC sides.

The coordination of DERs located in different subgrids is not fully explored in those aforementioned proposals. For instance, ESUs are more likely to be organized in multiple clusters which can be dispersedly deployed throughout the facility and connected to either DC or AC subgrids, and hence new clusters can be added to the system as the demanded storage capacity increases over time [12]. The MG control must ensure proper power sharing among the ESUs, nevertheless. Moreover, since mismatches between the ESUs can lead to SoC imbalance, which may degrade the storage system lifetime, the EMS must provide SoC equalization among distributed ESUs. Finally, it is important that the EMS considers the MG as a single-controllable entity, regulating the power exchanged with the mains, in order to mitigate the detrimental impact on the power system caused by heavy penetration of DERs.

To perform an EMS considering the features aforementioned, this paper uses the model-free power-based control (PBC) approach, which is based on a central controller that coordinately regulates the power flow of DERs dispersedly located in both subgrids. The PBC was initially proposed as a model-free approach to coordinatedly control DERs in single-phase AC MGs [13], and was then modified to control single- and three-phase DERs coexisting in three-phase AC MGs [14]. In [15], the PBC is used to control the active power in DC MGs, in which a power loop tracks a given power reference to maintain the DC bus voltage within acceptable ranges. The method proposed herein improves the PBC strategy to enable the management of ESUs dispersedly located in both subgrids, achieving proportional power sharing and SoC equalization, by considering the SoC of every ESU as part of the PBC.

In order to compare the previous literature with the proposed method, underlining the improved results achieved herein and its novelty, Table I summarizes the current state-of-the-art. Such comparison aims at highlighting the main features of each proposal in terms of: i) hybrid AC/DC MG acting as a single-controllable entity; ii) presence of ESUs in both subgrids; iii) grid-connected and islanded operating modes; iv) SoC equalization among ESUs located in both AC and DC subgrids; v) no need of previous knowledge of network parameters; vi) dispatchable grid power flow; and vii) plug-and-play capability. The proposed model-free method contributes to fulfil the gap of hybrid AC/DC MG control featuring grid power flow control and SoC balancing in both subgrids.

The paper is organized as follows: Section II presents the MG structure and describes the behavior of the IC and DERs during grid-connected and islanded modes. Section III presents the EMS and the local ESU energy management features that enable SoC balancing. Section IV describes the experimental hybrid AC/DC MG. Section V shows the experimental results while section VI concludes.

II. Hybrid AC/DC Microgrid Structure

Fig. 1 shows the hybrid AC/DC MG structure considered in this paper. It comprises an interlinking utility interface (IUI) converter, AC and DC loads, as well as multiple DERs (e.g., PV generators and ESUs), which are dispersedly located throughout the MG nodes. The ESUs provide dispatch capability to the MG, enabling ancillary services to be performed during grid-connected mode and supporting the MG operation in islanded mode. The IUI couples the AC and DC buses and also interfaces the MG to the mains. In this paper, a two-stage topology is considered, as shown in Fig. 2. The two-stage topology allows to decouple the control loop dynamics of the AC and DC sides, and allows to accommodate higher voltage ripples in the DC link without affecting the voltage waveform at the IUI output terminals.

The MG control architecture is divided into three hierarchical levels. The primary level manages basic and specific local functions, e.g., inner control loops, synchronization, islanding detection and local energy management. The secondary level is entitled to manage the power exchange between the MG buses and the grid, to attain proportional power sharing among DERs in both grid-connected and islanded modes, to perform SoC equalization among the ESUs, and finally to guarantee equalized SoC operation of ESUs under typical operational conditions. The tertiary level is responsible for the global interaction between the MGs PCC and external players - e.g., the utility operator - and to define the PCC power reference that is transmitted to the secondary level.

The secondary and tertiary control level features are performed by a central controller (CC) embedded in the IUI. The CC receives the DERs output status and coordinates their output power broadcasting reference commands to their local controller (LC). A centralized control approach provides an accurate and efficient way to perform energy management tasks [17], [18] and, as the information flows only in one direction at a time (from LC to CC or vice-versa), the communication channels do not operate overloaded [19].

A low-bandwidth communication infrastructure is employed for exchanging information among the MG elements, enabling the CC to be aware of the status and available capacity of each DER. The communication infrastructure has a reduced amount of data flowing through the communication channel which reduces its stress [20]. In case of communication failure, proportional power sharing and grid power flow control might be lost; however, the primary level still guarantees system operation within grid-code requirements and the MG stability is not compromised.

This article has been accepted for publication in a future issue of this journal, but has not been fully edited. Content may change prior to final publication. Citation information: DOI 10.1109/TIE.2020.2984993, IEEE Transactions on Industrial Electronics

TABLE I: Comparative summary of the literature review on hybrid AC/DC MG energy management systems

Ref.	MG type	MG acts as a single-unit	ESUs located in both subgrids	*SoC* balancing in both subgrids	MG op. in both modes	Grid power flow control	Need of prev. know.	Communication	P&P	Exp. results
[8]	AC/DC	✓	-	-	✓	-	✓	-	-	-
[7]	AC/DC	-	-	-	-	-	-	✓	-	✓
[9]	AC/DC	✓	-	-	✓	✓	-	✓	-	-
[10]	AC/DC	-	-	-	✓	-	✓	-	-	✓
[11]	AC/DC	-	✓	✓	-	-	✓	-	-	-
[16]	AC/DC	✓	✓	-	-	-	✓	✓	-	-
[14]	AC	✓	-	-	✓	✓	-	✓	✓	-
[15]	DC	✓	-	-	-	-	-	-	-	✓
Proposed method	AC/DC	✓	✓	✓	✓	✓	-	✓	✓	✓

P&P: Plug-and-Play capability

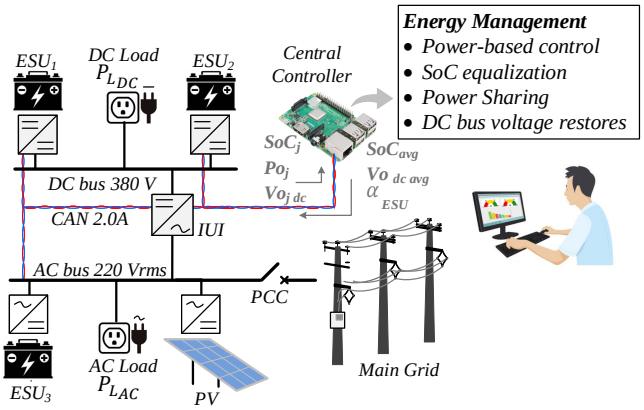

Fig. 1: Considered hybrid AC/DC microgrid structure.

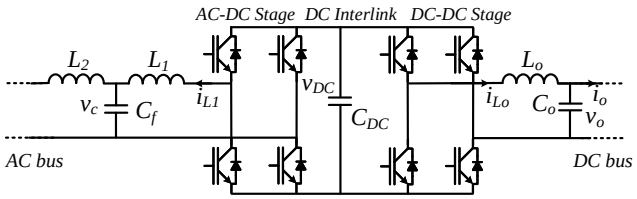

Fig. 2: Topology of the interlinking utility interface converter and interconnected subgrids.

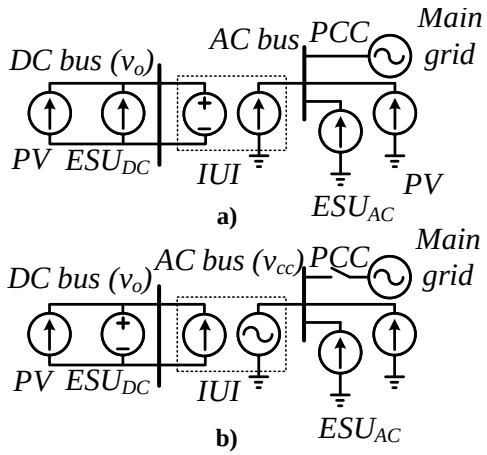

Fig. 3: Operating characteristics of converters in the hybrid AC/DC microgrid. **(a)** grid-connected mode; **(b)** islanded mode.

A. Primary Level Configuration of the Microgrid

To withstand system operation even without the coordination provided by the CC, the primary control level of the MG elements must be configured in a way that a grid-forming unit is always available in both AC and DC buses. Fig. 3 shows the IUI and DERs behavior during grid-connected and islanded modes. During the grid-connected mode, Fig. 3(a), the AC bus voltage and frequency references are enforced by the mains, thus, PVs and ESUs perform as controlled current sources, as well as the AC/DC stage of IUI that behaves as grid-following synchronized with the grid voltage. The active power exchanged by the IUI and the AC bus is defined by the local DC link control loop, which establishes the active power reference needed to maintain the DC link voltage regulated, while the reactive power loop is performed by sensing the grid current [21]. The DC/DC stage of IUI is controlled as a voltage source and regulates the DC bus voltage. Since the IUI DC/DC stage is seen as a perturbation for the converter DC link, the active power required by the DC/DC stage is delivered/absorbed by the AC/DC stage. In the DC side of the MG, PVs and ESUs also behave as controlled current sources.

During the islanded mode, Fig. 3(b), since the mains no longer provides voltage and frequency references for the AC bus, the AC/DC stage of the IUI is controlled as a voltage source, performing as a grid-forming converter and establishing voltage and frequency references to the whole AC MG. The DC/DC stage is then controlled as a current source, assuming the responsibility for the power balance through the IUI DC link. The DERs in the AC side still perform as current sources. The ESUs in the DC side perform as voltage sources regulating the DC bus voltage, whereas the PVs keep operating as current sources. The ESUs in the DC side follow DC-bus signaling, in which DC bus voltage level is divided into sectors that determine when ESUs shall operate in voltage- or current-controlled mode [22]. It is worth mentioning that the DERs in the AC side can be devised considering droop-control as in [23], or controlled as a voltage source by applying the triple-loop control as in [24], and then share the power contribution during sudden load changes with the IUI.

This article has been accepted for publication in a future issue of this journal, but has not been fully edited. Content may change prior to final publication. Citation information: DOI 10.1109/TIE.2020.2984993, IEEE Transactions on Industrial Electronics

III. Proposed Energy Management System

The proposed EMS is based on the PBC algorithm, which is a coordinated MG control strategy originally proposed for AC MGs, in which DERs contribute to the MG power needs in proportion to their available capability [13], [14]. Such proportionality is obtained by means of scaling coefficients that are calculated at the CC and broadcasted to all DERs. Thereupon, their individual power references are calculated at their LCs being proportional to their power capacity. The PBC is used because it does not need of previous knowledge of the MG electrical model, and it is able to promote proportional power sharing among DERs regardless of their location while regulating the grid power. Although, the PBC as originally proposed does not consider ESU equalization, neither its application for hybrid AC/DC MG.

For a hybrid AC/DC MG, such strategy must be adapted to handle the existence of the DC bus and its local resources, as well as to manage power equalization among ESUs located in different subgrids. The EMS proposed herein aims to perform the power management of the whole hybrid AC/DC MG as a single-controllable entity, achieving proportional power sharing among ESUs in both AC or DC sides with *SoC* equalization, controlling the reactive power injection from DERs in the AC side, and the grid power flow.

For the proposed EMS, it is considered that the PV generators operate at their MPP, whereas ESUs power is defined by the scalar coefficients broadcasted by the CC. In the AC subgrid, the required reactive power is shared among every DER (i.e., PV and ESU). The PBC operation considering *SoC* balancing is described as follows and its operation is summarized in Fig. 4:

1) at first activation of the MG control, the CC polls each DER connected to the communication network and registers its type (PV or ESU), location (DC or AC buses) and rated capacity. After registration is completed, the CC starts the first control cycle for the PBC. Periodically, the CC broadcasts a registration call, in order to register new DERs to the CC database and making possible the plug-and-play connection of new DERs.
2) at the beginning of each control cycle, *k*, the CC communicates with all registered DERs and gathers their status information about their operation and available capability:

- from the j-th PV, it is required its active and reactive output power (if in the AC side) [$P_{PVj}(k)$,$Q_{PVj}(k)$] and its converter power rating [A_{PVj}];
- from the i-th ESU, it is required its active and reactive (if in the AC side) output power [$P_{ESUi}(k)$, $Q_{ESUi}(k)$], its maximum and minimum power capacities [$P^{max}_{ESUi}(k)$, $P^{min}_{ESUi}(k)$], which refers to the maximum discharging and charging power, and its state-of-charge [$SoC_i(k)$] and its converter power rating [A_{ESUi}] ;
- from the IUI, it is required its output power [$P_{IUIm}(k)$, $Q_{IUIm}(k)$] and its converter power rating [A_{IUIm}];
- and from the grid side of the PCC, the grid active and reactive power [$P_{GRIDm}(k)$, $Q_{GRIDm}(k)$] are measured by the CC itself.

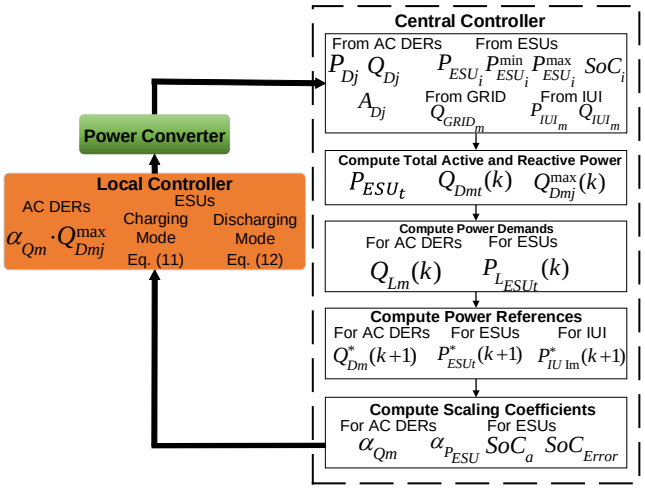

Fig. 4: Block diagram of the power-based control algorithm.

3) once all information is gathered, the PBC computes the status of the whole MG by means of quantities that are later described in eq. (4) and (5);
4) afterwards, the PBC determines the power needed from the DERs to achieve the desired grid power flow in the next control cycle (*k+1*) and computes the scalar coefficients that are broadcasted to every DER;
5) a scalar coefficient informs each DER about the ratio of its available active and/or reactive power to be exchanged with the MG, therefore, once the DER receives the coefficient from the CC, it updates its output power references and a new control cycle is initiated.

In step 1, the total active and reactive power delivered by DERs in the AC side along cycle k are computed in (1) and (2), respectively, while the maximum reactive power that each j-th DER is able to deliver is computed in (3). Note that J is the total number of PVs, while I is the total number of ESUs.

$$P_{Dtm}(k) = \sum_{i=1}^{I} P_{ESUim}(k) + \sum_{j=1}^{J} P_{PVjm}(k) \quad (1)$$

$$Q_{Dtm}(k) = \sum_{j=1}^{J} Q_{PVjm}(k) + \sum_{i=1}^{I} Q_{ESUim}(k) \quad (2)$$

$$Q^{max}_{Dj}(k) = \sqrt{A_{Dj}(k)^2 - P_{Dj}(k)^2} \quad (3)$$

In step 2, the CC computes the total active power in the whole MG, and the total reactive power absorbed within the MG AC bus, during cycle k, in (4) and (5), respectively.

$$P_{Ltm}(k) = P_{GRIDm}(k) + P_{Dtm}(k) \quad (4)$$

$$Q_{Ltm}(k) = Q_{GRIDm}(k) + Q_{Dtm}(k) + Q_{IUIm}(k) \quad (5)$$

Note that DERs not registered on the PBC (like non-dispatchable sources), and the distribution power losses in the line impedances are incorporated in $P_{Ltm}(k)$.

In step 3, the power references are calculated by the CC for the next control cycle $k+1$.

$$P^{*}_{ESUt}(k+1) = \sum_{m=1}^{3} [P_{Lm}(k) - P^{*}_{GRIDm}(k+1)] \quad (6)$$

$$Q^{*}_{Dtm}(k+1) = Q_{Lm}(k) - Q_{IUIm}(k) - Q^{*}_{GRIDm}(k+1) \quad (7)$$

This article has been accepted for publication in a future issue of this journal, but has not been fully edited. Content may change prior to final publication. Citation information: DOI 10.1109/TIE.2020.2984993, IEEE Transactions on Industrial Electronics

TABLE II: Scalling coefficients of power-based control

Power Conditions	Scalling Coefficients
$P^{min}_{ESUt}(k) \leq P^{*}_{ESUt}(k+1) \leq P^{max}_{ESUt}(k)$	$\alpha_{ESU} = \frac{P^{*}_{ESUt}(k+1)}{P^{max}_{ESUt}(k)}$
$P^{*}_{ESUt}(k+1) \leq P^{min}_{ESUt}(k)$	$\alpha_{ESU} = -1$
$P^{*}_{ESUt}(k+1) \geq P^{max}_{ESUt}(k)$	$\alpha_{ESU} = 1$
$-Q^{max}_{Dtm}(k) \leq Q^{*}_{Dtm}(k+1) \leq Q^{max}_{Dtm}(k)$	$\alpha_{Qm} = \frac{Q^{*}_{Dtm}(k+1)}{Q^{max}_{Dtm}(k)}$

where, $P^{*}_{ESUt}(k+1)$ defines the active power reference to be required from all ESUs. Such value cannot be superior to the maximum charge $[P^{min}_{ESUt}(k) = \sum_{i=1}^{I} P^{min}_{ESUi}(k)]$ and discharge $[P^{max}_{ESUt}(k) = \sum_{i=1}^{I} P^{max}_{ESUi}(k)]$ power capacities, to avoid overcharging or deep discharge of the battery banks, respectively. $P^{*}_{GRIDm}(k+1)$ and $Q^{*}_{GRIDm}(k+1)$ are the active and reactive grid power references.

In step 4, the CC computes the scaling coefficients and broadcasts them to DER's LCs which process the individual power references for each DER. The definition of the scaling coefficients is summarized in Table II. These coefficients are dimensionless, a factor which provides proportional power sharing among DERs considering their available capability. The reactive power of AC DERs is controlled by α_{Qm}, while ESU's active power is controlled by α_{ESU}. Whether the reactive power reference is negative or positive, the DER processes capacitive or inductive reactive power, respectively. In the same way, whether the ESU power reference is negative, positive or zero, the ESU operates in charging, discharging or idle-charge mode, respectively.

Besides the scalar coefficients, the CC also broadcasts the average SoC_a of the ESUs, which is calculated according to (8), where SoC_i is the SoC status of the *i*-th ESU. This information is employed by the LC to perform the *SoC* equalization process, which is described in Section III-A.

$$SoC_a = \frac{\sum_{i=1}^{I} SoC_i}{I} \tag{8}$$

The SoC equalization process of ESUs causes power imbalance among the ESUs that may exceed the rated power of their converters. To ensure that the converters of ESUs operate within their limits, and concomitantly achieve SoC equalization, the CC curtails α_{ESU} so that its value is lower than SoC_a. This limitation causes the power injected or absorbed by ESUs to be inferior to its maximum charging or discharging power capacity, while maintaining the power imbalance required to achieve the SoC equalization. In [25], it is also used a limiter in order to avoid high injected/absorbed power mismatching among dispersed ESUs, that could exceed their maximum acceptable power.

- In charging mode ($\alpha_{ESU} < 0$)
  If $|\alpha_{ESU}| > Soc_a$
$$\alpha_{ESU} = -SoC_a \tag{9}$$

- In discharging mode ($\alpha_{ESU} > 0$)
  If $|\alpha_{ESU}| > Soc_a$
$$\alpha_{ESU} = SoC_a \tag{10}$$

A. Local ESU Energy Management Strategy

Once α_{ESU} is calculated by the CC, it is then broadcasted to each ESUs LC that calculates its individual power reference. In a MG containing distributed ESUs, maintaining SoC balancing is important to improve the lifetime of the storage system. Thus, the EMS must provide means to equalize the SoC among ESUs [26]. The proposed local ESU energy management strategy provides a SoC equalization among ESUs independently of their location in a hybrid AC/DC MG.

The LC of ESUs weight the scaling coefficient in relation to their individual SoC_i and the system average SoC_a, transmitted by the CC by variable a_{pi}. This individual weight modifies locally the received α_{ESU} in a way that; during charging mode, the coefficient of an ESU is increased inversely to its SoC_i status, i.e., the ESU with the lowest *SoC* value will present the highest coefficient, while the ESU with the highest *SoC* value, the lowest coefficient. Therefore, units with lower stored energy absorb a greater share of the MG total charging power, leading to faster *SoC* growth. As the ESU's SoC_i approximates to the system average, the weight is reduced and the power imbalance introduced by this method is also decreased. Contrariwise, during the discharging mode, the weight value is greater for the ESUs with superior SoC_i values, whereas it is lower for the ESUs with inferior values of SoC_i. Thus, the units with greater amount of stored energy contribute more to the MG needs, and then they present faster *SoC* decrease. Again, as the ESU's SoC_i approximates to the system average, the weight value is reduced as well. In both cases, the SoC_i of every ESU tends to converge to the system average value over time.

The equalization speed is dependent on the mathematical function used to relate the scaling coefficient weight to the unit *SoC*. In the literature, *SoC* balancing has been addressed in droop controlled converters in which a droop adaptive function is introduced to modify the ESU output power in relation to its *SoC* status. In [26] and [25], a power function is employed, while [22] uses an exponential function to enforce *SoC* balancing. A comparative study among different compensation functions such as linear, power, exponential, hyperbolic sine and logarithmic to droop controlled ESUs is presented in [27]. The authors have concluded that the *power function* shows the fastest response in terms of equalization speed for the set of analyzed functions for both charging and discharging modes. Consequently, this paper considers a power function to compute the *SoC*-based scaling coefficient weight (i.e., a_{pi}). Therefore, the ESU power references are defined as:

- In charging mode
$$\begin{cases} P^{*}_{ESUi} = P^{min}_{ESUi} \cdot \alpha_{ESU} \cdot \alpha_{pi} \\ \alpha_{pi} = 1 + (SoC_a - SoC_i)^p \end{cases} \tag{11}$$

- In discharging mode
$$\begin{cases} P^{*}_{ESUi} = P^{max}_{ESUi} \cdot \alpha_{ESU} \cdot \alpha_{pi} \\ \alpha_{pi} = 1 - (SoC_a - SoC_i)^p \end{cases} \tag{12}$$

where the superscript p is a convergence factor that adjusts the equalization speed of *SoC* balancing. The higher the p, the faster the equalization procedure.

This article has been accepted for publication in a future issue of this journal, but has not been fully edited. Content may change prior to final publication. Citation information: DOI 10.1109/TIE.2020.2984993, IEEE Transactions on Industrial Electronics

TABLE III: Parameters of the hybrid AC/DC microgrid

MG Parameters	Value
Nominal bus voltage (DC, AC)	$380, 220\ V$
Nominal AC frequency	$60\ Hz$
PV power	$0.46\ kW$
Load power (DC, AC)	$1.9, 1.8\ kW$
IUI Converters Parameters	
Nominal power	$4.2\ kVA$
DC interlink (voltage, capacitance)	$600\ V, 3610\ \mu F$
LCL filter AC (L_1, L_2, C_f)	$430\ \mu H, 200\ \mu H, 10\ \mu F$
LC filter DC (L_o, C_o)	$1.25\ mH, 470\ \mu F$
ESUs Parameters	
Battery voltage	$48\ V$
Max. discharge power	$ESU_{1,2DC}$ $1.1\ kW$ ESU_{3AC} $0.55\ kW$
Max. charge power	$ESU_{1,2DC}$ $0.55\ kW$ ESU_{3AC} $0.275\ kW$
SoC limits (Max., Min.)	$1.0, 0.3$

During islanded mode, the ESUs in DC side behave as controlled-voltage sources, and they regulate the DC bus voltage. Simultaneously, they are power dispatchable DERs, and may keep the coordination among ESUs through an outer power loop (P^*_{ESUi}), whose output is added to the ESU output voltage set-point. In [23] and [24], a similar approach is explored to droop controlled inverters as a way to control the output power delivered by DERs. Section IV gives details of the MG setup and the implemented control scheme.

IV. Microgrid Setup

The proposed strategy is experimentally validated through the laboratory-scale prototype shown in Fig. 5. Its configuration and hierarchical control levels are shown in Fig. 1, while its parameters are shown in Table III. The hybrid AC/DC MG is composed of two ESUs in the DC side (i.e., ESU1 and ESU2), one ESU in the AC side (i.e., ESU3), one PV generator and one IUI converter which interlinks the two subgrids and the mains. The prototype is split into three parts: i) hardware; ii) control scheme; and iii) communication channel.

1) Hardware part: Both ESUs in the DC side are implemented by a dual active bridge (DAB) converter attached to a battery bank composed of four lead-acid 12V/110Ah batteries. The ESU in the AC side is devised by a back-to-back converter, which is linked to the AC bus at one side and to the grid on the other side through a transformer. The battery bank behavior is emulated digitally by an algorithm implemented in the converter's control. The PV generator comprises the solar array simulator E4360A connected to a PHB1500-CS grid-tied inverter. Finally, the IUI topology is shown in Fig. 2.

2) Control scheme: The control scheme is divided into three hierarchical levels as shown in Fig. 1. Fig. 6 shows the scheme of the primary control for the IUI converter that is composed of two distinct control structures, being able to operate in both grid-connected and islanded modes. In both modes, each converter stage (DC/DC and AC/DC) has two cascaded loops: an inner current control loop and an outer voltage control loop. During the grid-connected mode, the AC/DC stage operates controlling the DC interlink voltage

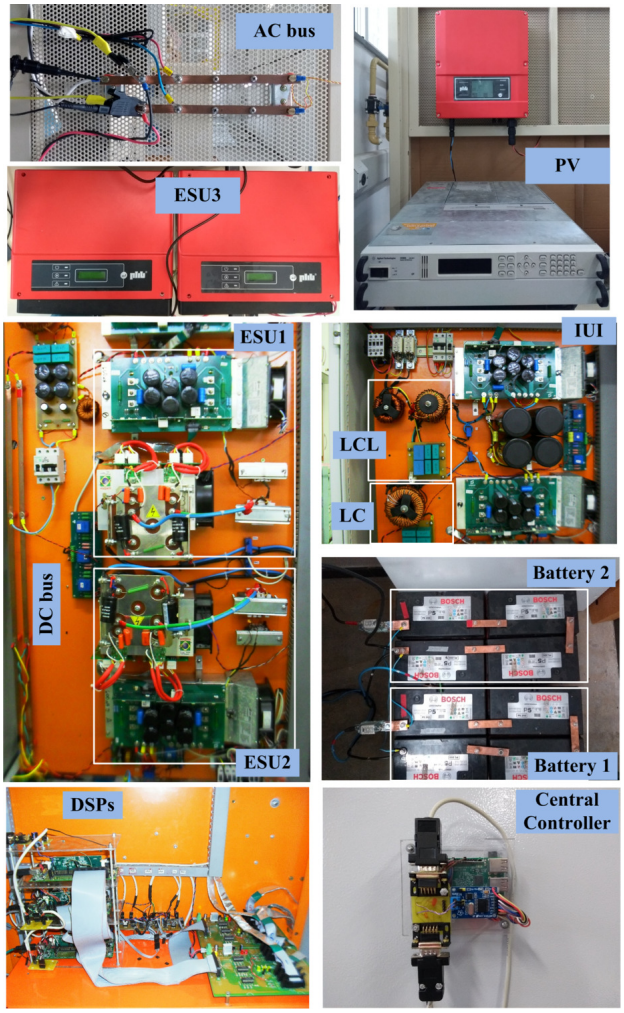

Fig. 5: Laboratory-scale prototype of the hybrid AC/DC microgrid.

(v_{DC}) that provides the reference current for the i_{L1} loop. In this operating mode, the stage AC/DC acts as a controlled current source at the AC side, and the DC/DC stage operates as a controlled voltage source regulating the DC bus voltage, in which the voltage loop employs the droop technique. During the islanded mode, the AC/DC stage operates as a controlled voltage source. Then, the voltage loop controls the voltage over C_f (v_c), providing the reference current to i_{L1} loop. The voltage loop in the DC/DC stage regulates the DC interlink voltage acting as a controlled current source at the DC bus, as described in Section II. In this control scheme, only the voltage loops change according to the operating mode.

Fig. 7 shows the scheme of the primary control for ESUs in the DC bus which is implemented to be able to control charge and discharge processes of batteries. Two control loops are implemented: a voltage droop controller that regulates the DC bus voltage, and a charge controller that regulates the absorbed current from ESUs during the charging mode. An inner current loop determines the operation mode of ESU, so that, during the discharging mode, the output of the voltage droop controller assumes the inductor current control, while in charging mode, the output of the charge controller regulates the inductor current.

Fig. 8 shows the scheme of the primary control for ESUs in

This article has been accepted for publication in a future issue of this journal, but has not been fully edited. Content may change prior to final publication. Citation information: DOI 10.1109/TIE.2020.2984993, IEEE Transactions on Industrial Electronics

the AC bus, that is based on a double-loop control of current and power loops. It is worth underlining that all the parameters related to the primary control level shown in Figs. 6, 7 and 8 are sized in the basis of local model in order to guarantee that the closed-loop behavior of the converters is stable and the paralleled connection of them in voltage mode does not lead to undesirable circulating currents.

The secondary control level is implemented in the CC that is embedded in a Raspberry Pi board. It is responsible for receiving the power status of all DERs, processing the PBC algorithm, broadcasting the scaling coefficients to ESUs LCs and adjusting the grid power reference according to the set-point provided by the tertiary control level. In addition to the CC function, Raspberry Pi is used as a datalogger, storing the power and voltage information from the converters.

3) Communication channel: The internal communication among the MG converters and the CC is provided by CAN communication bus. The implemented CAN protocol operates with a communication speed of 125 kbps. A data update time of 100 ms is chosen, so that the CAN bus is free for 66,9 ms between reception and data transmission by the CC. This guarantees the sending of other information and, in case of data loss, allows them to be forwarded.

V. Experimental Results

This section shows the experimental results obtained through a laboratory-scale hybrid AC/DC MG prototype operating in both grid-connected and islanded modes.

A. Grid-Connected Mode: SoC equalization

In grid-connected mode, it is analyzed the following conditions: i) equalization of ESUs during charge and discharge modes; ii) grid active power control; and iii) equalized operation under operational condition.

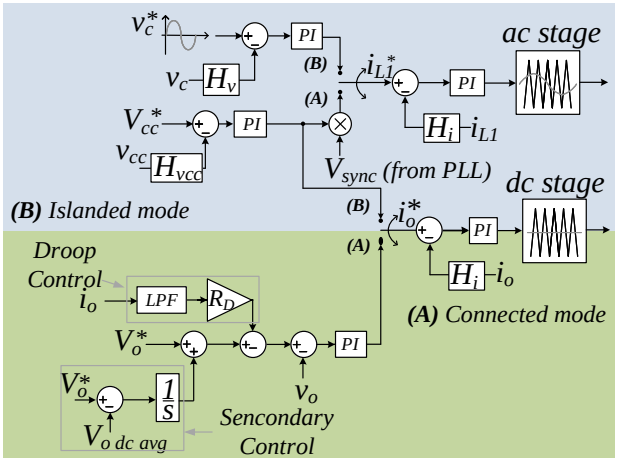

Fig. 6: Scheme of the primary control for the IUI converter; (A) grid-connected mode and (B) islanded mode.

Fig. 9 shows the system capability of changing from discharging to charging mode with SoC equalization. The initial $SoCs$ are: $SoC_1 = 0.85$, $SoC_2 = 0.75$ and $SoC_3 = 0.95$. The grid, load and PV powers are: $P_{GRID} = 1.2$kW, $P_{LOAD} = 2.67$kW and $P_{PV} = 0.46$kW. The convergence factor $p = 8$ is empirically chosen to enable the SoC equalization to be performed in one discharge cycle. ESUs operate in discharging mode with $\alpha_{ESU} = 0.36$, as shown in the bottom plot of Fig. 9. In this mode, the ESU with the highest SoC ($ESU_{3_{ca}}$) provides higher amount of power than the others, which is noticed by α_{p3} that is initially higher than the rest.

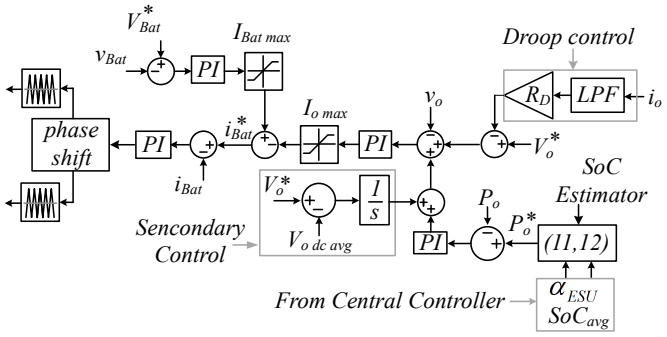

Fig. 7: Scheme of the primary control for ESUs in the DC subgrid.

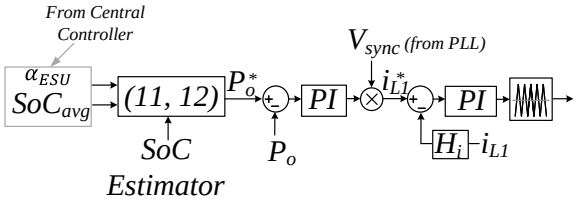

Fig. 8: Scheme of the primary control for the ESUs in the AC subgrid.

At $t = 245$min, it is applied a step change in the grid power reference (P^*_{GRID}), increasing it from 1.2kW to 2.9kW. At this instant, the ESUs change from discharging to charging mode, while the P_{GRID} follows its reference. The negative sign of α_{ESU} indicates power absorption. Note that, in both modes, proportional power sharing among ESUs is ensured to keep the $SoCs$ equalized, which is one of the goals of the proposed EMS. From Fig. 9 $P_{ESU_1} = P_{ESU_2} = 400$W and $P_{ESU_3} = 200$W in discharging mode; and $P_{ESU_1} = P_{ESU_2} = 260$W and $P_{ESU_3} = 130$W in charging mode, thus comparing to Table III one can note the proportional contribution of ESUs in both subgrids to their available discharging/charging power capacity. It can be seem from the Max. SoC deviation in Fig. 9 that during both operating modes SoC balancing is chased and once achieved, it is holded. The maximum SoC deviation is calculated as $Max.\ Soc\ deviation = (SoC_a\text{-}SoC_i)$.

B. Grid-Connected Mode: plug-and-play and communication failure

In grid-connected mode, it is analyzed the following conditions: i) MG behavior under communication channel failure; and ii) plug-and-play operation.

Fig. 10 analyzes the MG plug-and-play capability and its behavior under communication loss. The initial SoC of all ESUs are $SoC = 0.95$, while $P_{GRID} = 1.1$kW, $P_{LOAD} = 2.67$kW, and $P_{PV} = 0.46$kW. At $t = 65$min, ESU_3 is disconnected from the MG, and α_{ESU} immediately increases, hence ESU_1 and ESU_2 increase their power contribution but without compromising the SoC equalization between ESU_1 and ESU_2. At $t = 98$min, ESU_3 is reconnected and its SoC value tends to equalize with ESU_1 and ESU_2. α_{ESU} is

This article has been accepted for publication in a future issue of this journal, but has not been fully edited. Content may change prior to final publication. Citation information: DOI 10.1109/TIE.2020.2984993, IEEE Transactions on Industrial Electronics

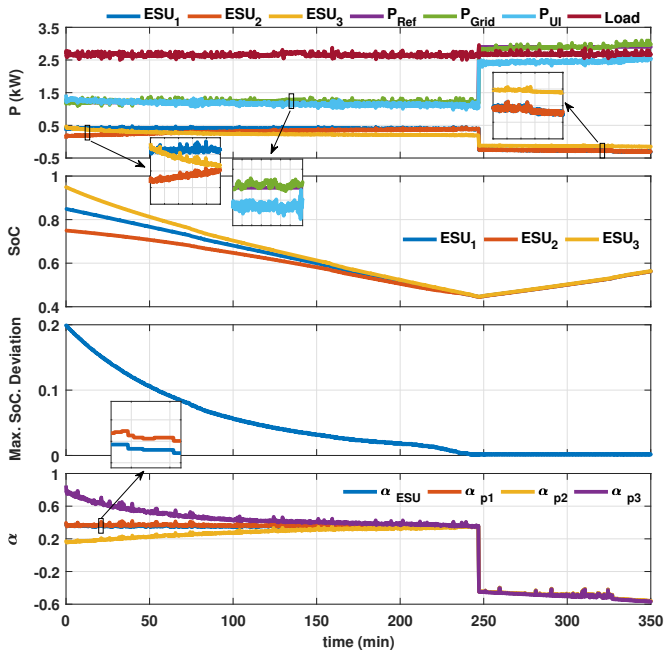

Fig. 9: MG operation with SoC equalization in grid-connected mode.

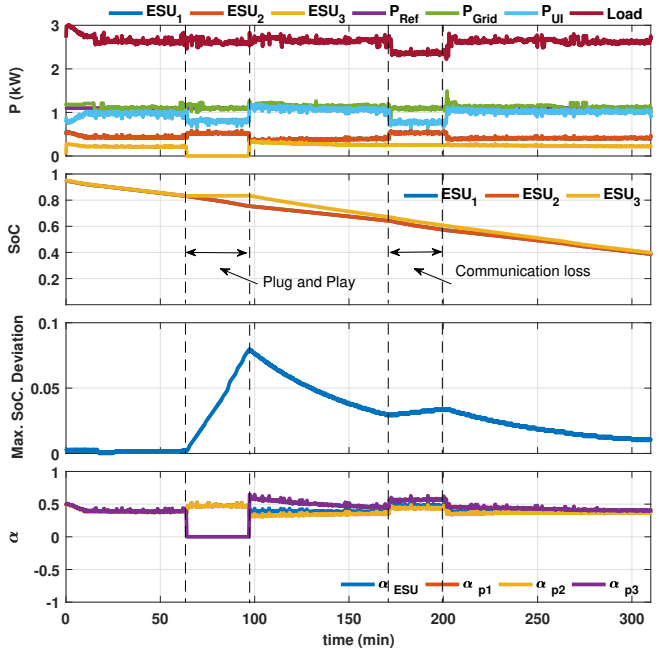

Fig. 10: MG operation with plug-and-play capability in grid-connected mode.

reduced because the demanded power is again divided among three ESUs. At $t = 172$min, the communication between ESU_3 and the CC is lost and its power measures are not received. The CC computes only ESU_1 and ESU_2 powers and α_{ESU} increases. However, ESU_3 injects a surplus power of 0.25kW into the MG, which reduces the perceived load power, P_L. At $t = 201$min, the communication channel is recovered and ESU_3 tends to equalize its SoC value with ESU_1 and ESU_2.

C. Islanded Mode

In islanded mode, the IUI converter operates as a grid-forming converter providing the AC voltage and frequency references for the MG, while the ESUs located in the DC subgrid regulate the DC bus voltage. Since $P_{GRID} = 0$kW, the ESUs and PVs are responsible for providing the load demand.

The following conditions are analyzed: i) equalization of ESUs in discharging mode; ii) bidirectional power flow capability of IUI converter; iii) grid-forming operation capability of IUI converter; and iv) capability of maintaining SoC equalization under load disturbances. The experimental result shown in Fig. 11 considers the following initial SoC values: $SoC_1 = 0.75$, $SoC_2 = 0.85$, $SoC_3 = 0.95$, while PV supplies 0.38kW, the initial DC load power is $P = 0.3$kW, and the initial AC load power is $P = 1.3$kW. It can be observed that the Max. SoC Deviation is steadily reduced during the process, the load power is proportionally shared among the ESUs: where $P_{ESU_1} = P_{ESU_2} = 550$W and $P_{ESU_3} = 275$W. Also, the IUI is capable of properly regulating the AC bus voltage and frequency, similarly as shown in Fig. 12. During the equalization process and the operation with the equalized SoC, the AC voltage shows THD value lower than 0.6%, and the AC and DC voltage magnitudes are 1.0p.u.

Initially in Fig. 11, all the loads are sited at the AC subgrid, thus the power flows from the DC to the AC side, and P_{IUI} value is negative. At $t = 97$min, the DC load is $P = 0.85$kW and the AC load is $P = 0.65$kW. In this condition, the power flowing through the IUI is approximately zero. At $t = 164$min, the AC load is $P_{L_{AC}} = 0$W and the DC load is $P_{L_{DC}} = 1.4$kW, thus the available power in the AC subgrid is transferred to the DC subgrid through the IUI. It confirms the bidirectional power flow capability of IUI converter.

In Fig. 12 are applied several load steps to verify whether the load disturbances cause deviation in the SoC equalization and in the DC voltage and AC frequency. The initial SoC values are: $SoC_1 = SoC_2 = SoC_3 = 0.95$, PV supplies 0.46kW and the initial DC load power is $P_{L_{DC}} = 0.3$kW, and the initial AC load power is $P_{L_{AC}} = 1.3$kW. The load power is proportionally shared among the ESUs: where $P_{ESU_1} = P_{ESU_2} = 540$W and $P_{ESU_3} = 270$W. Through the IUI converter, the power is transferred from DC to AC subgrid. At $t = 80$min, the DC load power is increased to $P_{L_{DC}} = 0.8$kW. At $t = 125$min, the DC load power is increased to $P_{L_{DC}} = 1.3$kW being equal to the AC load power and the power flowing through the IUI converter is approximately zero. At $t = 145$min, the DC load power is $P_{L_{DC}} = 2.3$kW and the AC load power is $P_{L_{AC}} = 0.65$kW. In this instant, the power flows from the AC subgrid to the DC subgrid. At $t = 165$min, the DC load power is $P_{L_{DC}} = 2.3$kW and the AC load power is $P_{L_{AC}} = 0$kW, and then the power flowing from AC to DC subgrid increases. Finally, at $t = 190$min, the DC load power is $P_{L_{DC}} = 0.3$kW and the AC load power is $P_{L_{AC}} = 0$W. In this instant, the PV is able to fully supply the loads and $P_{ESU_1} = P_{ESU_2} = P_{ESU_3} = 0$W. Thus, Fig. 12 shows that the load variations do not impair the equalization process and do not cause deviation in voltage and frequency higher than the limits imposed by grid-codes.

This article has been accepted for publication in a future issue of this journal, but has not been fully edited. Content may change prior to final publication. Citation information: DOI 10.1109/TIE.2020.2984993, IEEE Transactions on Industrial Electronics

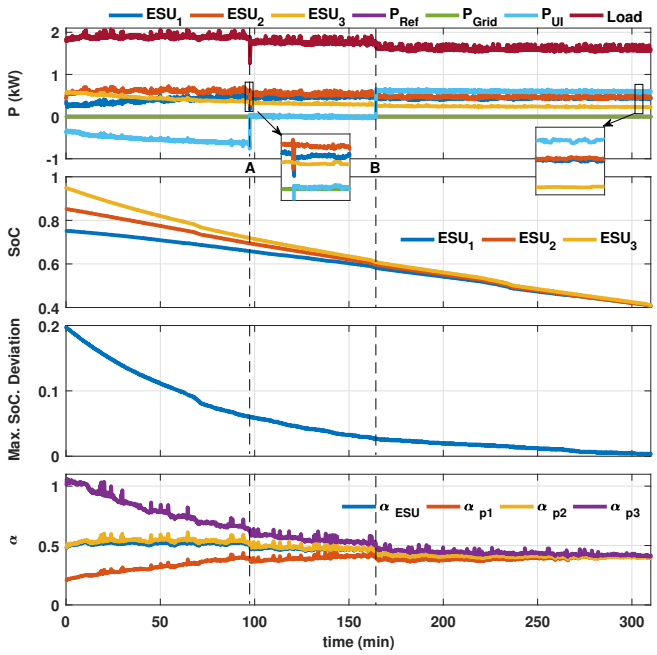

Fig. 11: MG operation with SoC equalization during islanded mode.

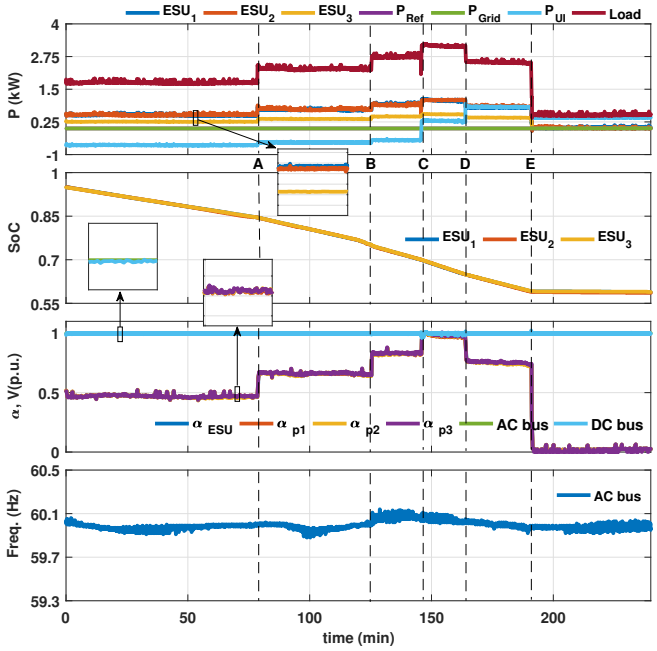

Fig. 12: MG operation under load variation during islanded mode.

VI. Conclusion

This paper proposed a model-free energy management system for hybrid AC/DC microgrid with *SoC* equalization of ESUs scatteredly distributed along AC and DC subgrids. The major objective of this paper is to achieve a proportional power sharing, *SoC* equalization among ESUs distributed in both AC and DC subgrids, and grid power flow control considering the hybrid AC/DC microgrid as a single-controlled entity. To achieve these objectives, a centralized power-based control is used. The power-based control coordinates the active power among the ESUs ensuring proportional power sharing; provides *SoC* equalization and controls the grid active power. The central controller relies on a low-bandwidth communication link and does not require previous knowledge of the microgrid parameters. The proposed strategy was experimentally validated and the results show that the main objectives were satisfactorily achieved in both grid-connected and islanded operating modes. Future works will be addressed to mitigate the impact of centralized communication infrastructure and to include battery bank of different technologies.

References

[1] Torquato, Ricardo and Salles, Diogo and Pereira, Caio Oriente and Meira, Paulo Cesar Magalhaes and Freitas, Walmir, "A comprehensive assessment of PV hosting capacity on low-voltage distribution systems," *IEEE Trans. Power Del.*, vol. 33, no. 2, pp. 1002–1012, 2018.

[2] Ismael, Sherif M and Aleem, Shady HE Abdel and Abdelaziz, Almoataz Y and Zobaa, Ahmed F, "State-of-the-art of hosting capacity in modern power systems with distributed generation," *Renewable energy*, vol. 130, pp. 1002–1020, 2019.

[3] S. Kotra and M. K. Mishra, "A supervisory power management system for a hybrid microgrid with hess," *IEEE Trans. Ind. Electron.*, vol. 64, DOI 10.1109/TIE.2017.2652345, no. 5, pp. 3640–3649, May. 2017.

[4] T. Dragičević, X. Lu, J. C. Vasquez, and J. M. Guerrero, "Dc microgridspart i: A review of control strategies and stabilization techniques," *IEEE Trans. Power Electron.*, vol. 31, DOI 10.1109/TPEL.2015.2478859, no. 7, pp. 4876–4891, Jul. 2016.

[5] Y. Xia, W. Wei, M. Yu, X. Wang, and Y. Peng, "Power management for a hybrid ac/dc microgrid with multiple subgrids," *IEEE Trans. Power Electron.*, vol. 33, DOI 10.1109/TPEL.2017.2705133, no. 4, pp. 3520–3533, Apr. 2017.

[6] J. M. Guerrero, J. C. Vasquez, J. Matas, L. G. de Vicuna, and M. Castilla, "Hierarchical control of droop-controlled ac and dc microgridsa general approach toward standardization," *IEEE Trans. on Ind. Electron.*, vol. 58, DOI 10.1109/TIE.2010.2066534, no. 1, pp. 158–172, Jan. 2011.

[7] A. A. A. Radwan and Y. A.-R. I. Mohamed, "Networked control and power management of ac/dc hybrid microgrids," *IEEE Syst. J.*, vol. 11, DOI 10.1109/JSYST.2014.2337353, no. 3, pp. 1662–1673, Sept. 2017.

[8] N. Eghtedarpour and E. Farjah, "Power control and management in a hybrid ac/dc microgrid," *IEEE Trans. Smart Grid*, vol. 5, DOI 10.1109/TSG.2013.2294275, no. 3, pp. 1494–1505, May. 2014.

[9] S. Kotra and M. K. Mishra, "Energy management of hybrid microgrid with hybrid energy storage system," in *2015 International Conference on Renewable Energy Research and Applications (ICRERA)*, vol. 1, DOI 10.1109/ICRERA.2015.7418532, pp. 856–860. IEEE, Nov. 2015.

[10] P. Wang, C. Jin, D. Zhu, Y. Tang, P. C. Loh, and F. H. Choo, "Distributed control for autonomous operation of a three-port ac/dc/ds hybrid microgrid," *IEEE Trans. Ind. Electron.*, vol. 62, DOI 10.1109/TIE.2014.2347913, no. 2, pp. 1279–1290, Feb. 2014.

[11] Z. Lv, P. Yang, Y. Xia, M. Yu, and W. Wei, "State of charge based decentralized coordination control for multiple bidirectional power converters in a hybrid ac/dc microgrid," in *2018 IEEE 8th Annual International Conference on CYBER Technology in Automation, Control, and Intelligent Systems (CYBER)*, vol. 1, DOI 10.1109/CYBER.2018.8688165, pp. 1456–1460. IEEE, 2018.

[12] J. M. Guerrero, P. C. Loh, T.-L. Lee, and M. Chandorkar, "Advanced control architectures for intelligent microgrids - part ii: Power quality, energy storage, and ac/dc microgrids," *IEEE Trans. Ind. Electron.*, vol. 60, DOI 10.1109/TIE.2012.2196889, no. 4, pp. 1263–1270, Apr. 2013.

[13] T. Caldognetto, S. Buso, P. Tenti, and D. I. Brandao, "Power-based control of low-voltage microgrids," *IEEE Journal of Emerging and Selected Topics in Power Electronics*, vol. 3, DOI 10.1109/JESTPE.2015.2413361, no. 4, pp. 1056–1066, Dec. 2015.

[14] D. I. Brandao, L. S. de Araújo, T. Caldognetto, and J. A. Pomilio, "Coordinated control of three-and single-phase inverters coexisting in low-voltage microgrids," *Applied Energy*, vol. 228, DOI 10.1016/j.apenergy.2018.07.082, pp. 2050–2060, Jul. 2018.

[15] G. Liu, T. Caldognetto, P. Mattavelli, and P. Magnone, "Power-based droop control in dc microgrids enabling seamless disconnection from upstream grids," *IEEE Trans. Power Electron.*, vol. 34, DOI 10.1109/TPEL.2018.2839667, no. 3, pp. 2039–2051, Mar. 2018.

[16] M. Hosseinzadeh and F. R. Salmasi, "Robust optimal power management system for a hybrid ac/dc micro-grid," *IEEE Trans. on Sustain. Energy*, vol. 6, DOI 10.1109/TSTE.2015.2405935, no. 3, pp. 675–687, Jul. 2015.

[17] J. Xiao, P. Wang, and L. Setyawan, "Hierarchical control of hybrid energy storage system in dc microgrids," *IEEE Trans. Ind. Electron.*, vol. 62, DOI 10.1109/TIE.2015.2400419, no. 8, pp. 4915–4924, Aug. 2015.

[18] M. N. Ambia, A. Al-Durra, and S. Muyeen, "Centralized power control strategy for ac-dc hybrid micro-grid system using multi-converter scheme," in *IECON 2011-37th Annual Conference of the IEEE Industrial Electronics Society*, DOI 10.1109/IECON.2011.6119420, pp. 843–848. IEEE, 2011.

[19] T. L. Vandoorn, J. C. Vasquez, J. De Kooning, J. M. Guerrero, and L. Vandevelde, "Microgrids: Hierarchical control and an overview of the control and reserve management strategies," *IEEE Ind. Electron. M.*, vol. 7, DOI 10.1109/MIE.2013.2279306, no. 4, pp. 42–55, Dec. 2013.

[20] X. Lu, J. M. Guerrero, K. Sun, and J. C. Vasquez, "An improved droop control method for dc microgrids based on low bandwidth communication with dc bus voltage restoration and enhanced current sharing accuracy," *IEEE Trans. Power Electron.*, vol. 29, DOI 10.1109/TPEL.2013.2266419, no. 4, pp. 1800–1812, Apr. 2013.

[21] P. Tenti, T. Caldognetto, S. Buso, and D. I. Brandao, "Control of utility interfaces in low-voltage microgrids," *Brazilian Power Electronics Journal*, vol. 20, DOI 10.1109/PEDG.2014.6878674, no. 4, pp. 373–382, Nov. 2015.

[22] T. R. Oliveira, W. W. A. G. Silva, and P. F. Donoso-Garcia, "Distributed secondary level control for energy storage management in dc microgrids," *IEEE Trans. Smart Grid*, vol. 8, DOI 10.1109/TSG.2016.2531503, no. 6, pp. 2597–2607, Nov. 2017.

[23] Lissandron, Stefano and Mattavelli, Paolo, "A controller for the smooth transition from grid-connected to autonomous operation mode," in *2014 IEEE Energy Conversion Congress and Exposition (ECCE)*, pp. 4298–4305, 2014.

[24] Buso, Simone and Caldognetto, Tommaso and Liu, Qing, "Analysis and experimental characterization of a large-bandwidth triple-loop controller for grid-tied inverters," *IEEE Trans. Power Electron.*, vol. 34, no. 2, pp. 1936–1949, 2018.

[25] X. Lu, K. Sun, J. M. Guerrero, J. C. Vasquez, and L. Huang, "Double-quadrant state-of-charge-based droop control method for distributed energy storage systems in autonomous dc microgrids." *IEEE Trans. Smart Grid*, vol. 6, DOI 10.1109/TSG.2014.2352342, no. 1, pp. 147–157, Jan. 2015.

[26] N. L. Díaz, A. C. Luna, J. C. Vasquez, and J. M. Guerrero, "Centralized control architecture for coordination of distributed renewable generation and energy storage in islanded ac microgrids," *IEEE Trans. Power Electron.*, vol. 32, DOI 10.1109/TPEL.2016.2606653, no. 7, pp. 5202–5213, Jul. 2017.

[27] F. L. Marcelino, H. H. Sathler, W. W. A. G. Silva, T. R. de Oliveira, and P. F. Donoso-Garcia, "A comparative study of droop compensation functions for state-of-charge based adaptive droop control for distributed energy storage systems," in *Power Electronics for Distributed Generation Systems (PEDG), 2017 IEEE 8th International Symposium on*, DOI 10.1109/PEDG.2017.7972492, pp. 1–8. IEEE, Apr. 2017.